Structural insight into the interaction of O-acetylserine sulfhydrylase with competitive, peptidic inhibitors by saturation transfer difference-NMR

R. Benoni, T.A. Pertinhez, F. Spyrakis, S. Davalli, S. Pellegrino, G. Paredi, A. Pezzotti, S. Bettati, B. Campanini and A. Mozzarelli Structural insight into the interaction of *O*-acetylserine sulfhydrylase with competitive, peptidic inhibitors by Saturation Transfer Difference-NMR. FEBS LETTERS. 2016, 590 pp: 943-953.

DOI: 10.1002/1973-3468.12126

Structural insight into the interaction of *O*-acetylserine sulfhydrylase with competitive, peptidic inhibitors by Saturation Transfer Difference-NMR

R. Benoni[1,#], T.A. Pertinhez[2,#], F. Spyrakis[3], S. Davalli[4], S. Pellegrino[5], G. Paredi[6], A. Pezzotti[6], S. Bettati[1,7], B. Campanini[6,*] and A. Mozzarelli[6,7,8]

[1]Dept. Neurosciences, University of Parma, Parma; [2]Dept. Oncology and Advanced Techniques, Arcispedale Santa Maria Nuova-IRCCS, Reggio Emilia; [3]Dept. Food Sciences, University of Parma, Parma, *Current address*: Dept. Life Sciences, University of Modena and Reggio Emilia, Modena; [4]Aptuit, Medicine Research Center, Verona; [5]Dept. Pharmaceutical Sciences, Section of General and Organic Chemistry "A. Marchesini", University of Milan, Milan; [6]Dept. Pharmacy, University of Parma, Parma; [7]National Institute for Biostructures and Biosystems, Rome; [8]Institute of Biophysics, CNR, Pisa, Italy.

[#] these authors contributed equally to the work.
*Address correspondence to: Barbara Campanini, Dipartimento di Farmacia, Università degli Studi di Parma, Parco Area delle Scienze 23/A, 43124 Parma, Italy. E-mail: barbara.campanini@unipr.it. Phone: +39 0 521 906 613, fax: +39 0 521 905 151.

Abstract
O-acetylserine sulfhydrylase (OASS), the enzyme catalyzing the last step of cysteine biosynthesis in bacteria, is involved in antibiotic resistance and biofilm formation. Since mammals lack OASS, it is a potential target for antimicrobials. However, a limited number of inhibitors has been developed and crystallized in complex with OASS. STD-NMR was applied to study the interaction of the inhibitory pentapeptide MNYDI with the CysK and CysM OASS isozymes from *Salmonella typhimurium*. Results are in excellent agreement with docking and SAR studies and confirm the important role played by the C-terminal Ile5 and the arylic moiety at P3 in dictating affinity.

Keywords:
Cysteine biosynthesis
Cysteine synthase
CysK
CysM
Saturation Transfer Difference NMR

Abbreviations:
GEM, Group Epitope Mapping; CysK, *O*-acetylserine sulfhydrylase-A; CysM, *O*-acetylserine sulfhydrylase-B; OASS, *O*-acetylserine sulfhydrylase; PLP, pyridoxal 5'-phosphate; CysE, serine acetyltransferase; STD-NMR, Saturation Transfer Difference-NMR; ASTD, STD amplification factor; MIFs, Molecular Interaction Fields.

Highlights:

- Cysteine can be synthesized in bacteria by either one of the two isozymes CysK and CysM
- STD-NMR allows to study protein-ligand binding specificity in solution
- Peptidic inhibitors of the two isozymes with MNX_1X_2I sequence have been developed
- An arylic substituent at position X_1 improves affinity for CysK
- The N-terminal amino acids dictate the specificity for CysM

Introduction

The pyridoxal 5'-phosphate-dependent enzyme *O*-acetylserine sulfhydrylase (OASS) catalyses the last step of the reductive sulfate assimilation pathway and has been identified in bacteria, protozoa, mycobacteria and plants [1-6]. Different isoforms of OASS are differentially expressed depending on growth conditions, with at least two isoforms being identified for each organism [4, 7-10]. Most proteobacteria, including *Salmonella enterica* serovar Typhimurium and *Haemophilus influenzae*, express the CysK and CysM isoforms, that share a very similar three-dimensional structure and a 70% sequence identity for residues in the active site [11, 12]. Both isozymes can synthesize cysteine from *O*-acetylserine and bisulfide (Figure 1) but CysM, owing to a larger active site, can also use thiosulfate as nucleophile [13, 14]. Under basal growth conditions CysK is largely over-expressed with respect to CysM, whose expression is possibly triggered by anaerobiosis [14, 15]. However, little is known about the differential expression of the two isoforms during physiologically-relevant processes like infection and long-term survival [16]. CysK activity within the bacterial cell is inhibited by CysE, the enzyme that catalyzes the previous step in the reductive sulfate assimilation pathway, i.e. L-serine activation to *O*-acetylserine [17]. CysE binds at CysK active site to form a stable complex with a dissociation constant in the low nM range [18-22]. The recognition element of CysE is the C-terminus that penetrates with the last five amino-acids (MNLNI in the case of *H. influenzae)* in CysK active site. While the function and structure of OASS have been thoroughly investigated, the intricate metabolic and regulatory networks in which OASS is involved are only recently being unveiled [23], finding that they encompass the activation of a toxin involved in contact dependent growth-inhibition [24] and biofilm formation [25]. Therefore, specific CysK/CysM inhibitors represent not only research tools but also potential innovative antibiotics that might interfere with the ability of bacteria to perform essential functions for infection and long-term survival [26, 27]. Unfortunately, only a limited number of specific, low-affinity inhibitors of either CysK or CysM has been identified to date [4, 11, 26, 28-37], and for an even smaller number of them three-dimensional structures of complexes with the enzyme are available [19, 34, 35]. Of these none pertains to CysM isozyme, an apparently harder target, for which no high-affinity ligands have been identified yet [11, 36]. The most extensive study on the structure-activity relationship (SAR) of inhibitors directed to CysK and CysM from *S. Typhimurium* (StCysK, StCysM) was carried out using a small library of pentapeptides and a mixed experimental and virtual-screening approach [11, 35, 36]. Two main findings arose: i) the occupation of a small hydrophobic pocket in the active site, also identified in Mycobacterium CysK [31], is essential for high-affinity binding to CysK [11, 36]; ii) the selectivity for CysK/CysM is dictated by the two N-

terminal residues of the peptide that protrude outside the OASS active site and that were not visible in the crystal structures of CysK solved to date [19, 35, 36].

Saturation Transfer Difference (STD)-NMR is an NMR technique that measures the saturation transferred from a protein to its bound ligand, and allows the determination of the spatial proximity between the functional groups on a ligand and the protein matrix within a binding site [38]. In this work the complex between MNYDI and HiCysK, for which the three-dimensional structure has been solved [35], was first analyzed by STD-NMR. The approach was subsequently used to characterize the interaction of either StCysK or StCysM with MNYDI, a pentapeptide identified as a high affinity OASS ligand by a computational-experimental analysis of an *in silico*-generated library [35]. The experimental data are in excellent agreement with docking poses and confirm previous SAR studies. This method can be applied to the screening of peptide-mimetic libraries for the identification of specific or dual CysK/CysM inhibitors, and for ligand optimization.

Materials and Methods

Protein expression and purification. HiCysK, StCysK and StCysM were expressed and purified as previously described [18, 22, 36]. The N-terminal His-tag was removed and protein purity was higher than 98%. The specific activity was comparable to that of previous preparations [8].

Peptide synthesis. The peptide (MNYDI) was prepared by microwave-assisted solid phase synthesis [39] based on Fmoc chemistry on preloaded Wang resin (0.7 meq/g substitution), using a fivefold molar excess of 0.2 M Fmoc-protected amino acids dissolved in N-methyl pyrrolidinone, and using HOBT/HBTU/DIEA (5 : 5 : 10 eq) as activators. Coupling reactions were performed for 5 min at 40 W with a maximum temperature of 75 °C. Deprotection was performed in two stages using 20% piperidine in dimethylformamide (5 and 10 min each). Cleavage was performed using 10 mL of Reagent K (trifluoroacetic acid/phenol/water/thioanisole/ 1,2-ethanedithiol; 82.5 : 5 : 5 : 5 : 2.5) for 180 min. Following cleavage, the peptide was precipitated and washed using ice-cold anhydrous ethyl ether. The peptide was purified by RP-HPLC using a gradient elution of 5–70% solvent B (solvent A: water/acetonitrile/trifluoroacetic acid 94.9 : 5 : 0.1; solvent B: water/acetonitrile/trifluoroacetic acid 5 : 94.9 : 0.1) over 20 min at a flow rate of 10 mL/min^{-1}. The purified peptide was freeze-dried and stored at 0 °C. The identity of the peptide was assessed by MS/MS analysis using a 4800 MALDI TOF/TOF ABSciex mass spectrometer and NMR (vide infra).

Binding studies. The dissociation constant of MNYDI peptide to the enzyme isoforms was previously determined in Hepes buffer [36]. The peptide dissociation constant was re-measured in a solution containing 5 mM phosphate buffer, pH 8.0, the buffer used for STD-NMR measurements (see below). The binding of peptide to the enzyme isoforms was determined by monitoring the increase in fluorescence emission of PLP at 500 nm following excitation at 412 nm [18, 35].

NMR Spectroscopy. All NMR spectra were recorded at 20 °C on a Varian INOVA 600AS spectrometer operating at 599.730 MHz for the ^{1}H frequency. Proton assignment of free MNYDI was carried out on a solution containing 3 mM peptide, 5% D_2O/95% phosphate buffer, pH 4.0. The two-dimensional ^{1}H homonuclear, TOCSY and ROESY, experiments were performed using the standard pulse sequences [40] and proton chemical shifts were referenced to water signal. Data were processed using NMRPipe/NMRView programs [41, 42]. The spin systems were identified,

and the sequential assignment was obtained using the standard method [43]. The assignments were confirmed at pH 8.0, under the same experimental conditions of binding experiments.

STD-NMR. Saturation transfer-difference experiments were performed on solution containing 6.7 μM enzyme and 2 mM MNYDI peptide (molar ratio of enzyme/peptide equal to 1:300), 5 mM phosphate buffer, 5% D_2O, at pH 8.0. NMR spectra were acquired with 32k data points and 3500 scans in a spectral window of 9000 Hz. The water signal suppression was achieved by the excitation sculpting method (dpfgse-water) [44].

For selective saturation, a train of Gaussian shaped pulses with a length of 30 ms and 46 dB of attenuation were employed, with an inter-pulse delay of 1 ms for a saturation time of 3 s. The irradiation field strength was 81.5 Hz. Selective saturation of the proton resonances (on-resonance) was performed by selective irradiation at frequency – 0.2 ppm, while for the reference spectrum (off-resonance) the samples were irradiated at 26.6 ppm. The protein signals were suppressed by a 10 ms T1ρ-spinlock. The spectra were processed and analyzed using MestReNova 8.1 software.

STD experiments were optimized for the enzyme StCysM (1D spectrum, figure 1S). The enzyme upfield signal (-0.2 ppm) is relatively close to the peptide methyl protons. To eliminate the partial contribution of the peptide saturation, STD spectra of MNYDI and the MNYDI/enzyme complexes were acquired under the same experimental conditions, and the STD spectra of MNYDI was subtracted from the STD-NMR spectra of the complexes.

To derive the ligand Group Epitope Mapping (GEM), the STD amplification factor (ASTD) was calculated as:

$$ASTD = I_{STD} / I_0 * MR$$

The saturation of individual protons was normalized using the highest saturated signal as 100% to generate GEM and derive information of the proximity of each proton to the surface of protein binding pocket.

Molecular modelling. Docking simulations were performed as previously described [36]. Molecular Interaction Fields (MIF) were calculated with GRID implemented in the FLAP software [45], developed and licensed by Molecular Discovery Ltd. (www.moldiscovery.com). The DRY probe was used to describe hydrophobic regions within the binding site, while the O (sp2 carbonyl oxygen) and N1 (neutral amino nitrogen) probes were used to identify H-bond acceptor and donor regions, respectively.

Results and Discussion

The complex between MNYDI peptide and HiCysK was previously studied by fluorescence spectroscopy and protein crystallography [35] and was used as a model for setting up the STD-NMR experiments with StCysK and StCysM. MNYDI peptide interacts with HiCysK active site mainly through H-bonds involving its C-terminal carboxylate and hydrophobic interactions involving the side chains of Ile5 and Tyr3 (Figure 2a). The dissociation constant of MNYDI for either CysK or CysM was measured in phosphate buffer, i.e. the buffer used for STD-NMR measurements, because anions, like sulfate, significantly reduce the affinity of peptides for CysK [35]. A representative fluorimetric titration of HiCysK with MNYDI is reported in Figure 2b,c and the dissociation constants are reported in Table 1. The affinity of MNYDI falls within a range that allows to carry out STD-NMR experiments, as the efficiency of the saturation transfer to the ligand depends on its off-rate, i.e. a fast chemical exchange is required to collect spectra with a good signal-to-noise ratio [46, 47]. The ^{1}H chemical shifts of MNYDI peptide were attributed as reported in Table 2. The saturation frequency of on-resonance spectra is close to the peptidic ligand resonances. To overcome this problem the on-resonance spectrum of the peptide alone was acquired and a correction in the calculation of the saturation transfer (ASTD) and Group Epitope Mapping (GEM) was applied. The STD difference spectrum of the HiCysK:MNYDI complex is reported in Figure 3. The observed resonances arise from the saturation of the ligand bound to the enzyme and the subsequent dissociation, which transfers this saturation into solution. To gain information on the binding mode of the peptide and the proximity of each proton to the interacting protein surface, the GEM was calculated for each proton from the STD spectrum (Figure S2), as reported in Figure 4. The saturation of individual protons was normalized to the highest saturated proton in the peptide. For all the three complexes the highest saturated proton belongs to the C-terminal Ile (Ile5), in particular to the βH (StCysM) or to the γ_1H (StCysK, HiCysK). This finding is in excellent agreement with previous structural, computational and functional data [4, 19, 20, 35, 48]. A distinguishing feature of StCysK:MNYDI complex is a high saturation of the arylic protons that reaches 64% of GEM in the case of StCysK δH of Tyr3. This is also in agreement with previous SAR analysis [11, 35] that attributed to an aromatic residue at position P3 a high contribution to peptide binding to StCysK.

In order to interpret the GEM signals, we took advantage of previous Molecular Modelling studies carried out on thirteen peptides interacting with HiCysK, StCysK and StCysM [36]. The predicted poses for the MNYDI peptide within the protein binding site, shown in Figure 5, are in strong agreement with the GEM signals. The fundamental role played by Ile5 in stabilizing the protein-peptide interaction is evident in the three complexes, being the amino acid deeply buried within the

binding site. The Ile5 orientation is maintained in the three complexes, with the terminal carboxylic group interacting with T69, N72, T73, Q143 in HiCysK, with the corresponding T68, N71, T72, Q142 in StCysK, and with T68, G70, T72 and Q140 in StCysM. As previously reported [20, 35, 36], the energetic contribution of the interaction provided by Ile5 seems to be the most important, in particular for CysM (Figure 5c), where the residues contributes by itself for more than 50% in GEM. This difference with respect to CysK might be due to the presence of R210 side chain, a residue absent in CysK, that directly points towards the interior of the pocket. R210, replacing G230 in StCysK, also contributes to increase the polarity of StCysM binding site, generating a H-bond donor contour in correspondence to Ile5 hydrophobic side-chain (red contour in Figure 6c) and, likely, to decrease the affinity of MNYDI towards the protein. Asp4 occupies a similar position in the three analyzed complexes. In HiCysK binding site Asp4 forms favourable interactions by contacting S70 through the side-chain carboxylic group, and G71 with the backbone carbonyl. The hydrogen atoms located on the β-carbon are distant from the residues lining the pocket, as well as the backbone amino hydrogen, which might justify the poor and absent corresponding GEM signal. Similar interactions are maintained within StCysK binding site with S69 and G70 and, in agreement, a comparable GEM signal was registered. In StCysM the Asp4 carboxylic side-chain mainly contacts S69 and R99 and, reasonably, gives a similar GEM signal. Tyr3 shows very different orientations in the three complexes (Figure 5), in particular in HiCysK and StCysK binding sites. In the HiCysK-peptide complex, Tyr3 is oriented towards the domain interface possibly making π-π interactions with F144, to which the positive δH and εH GEM signals might be attributed. No direct hydrogen bond is formed by the side-chain hydroxyl group. In the StCysK-peptide model the residue side-chain is able to directly H-bond R99, being oriented towards the opposite domains interface crevice. Interestingly, when docked in StCysM binding site, Tyr3 assumes an orientation more similar to that proposed in the HiCysK-peptide complex, forming an H-bond with E120 and possibly making π-cation interactions with R210. The peculiar arrangement assumed by Tyr3 in the StCysK-peptide complex might explain the higher GEM signal registered for this interaction with respect to the other two complexes, in particular for the aromatic hydrogen atoms. Lower signals are reasonably generated by Asn2 and Met1, being the two terminal residues more solvent exposed and, consequently, more flexible with respect to the previous ones. For instance, no specific contact is formed by Asn2 in HiCysK and a single H-bond with I229 backbone is observed in StCysK. Differently, in StCysM multiple H-bond interactions are made by Asn2 side-chain with S205 side-chain and I206 and I209 backbone carbonyl groups. This would likely imply a higher complex stability, supporting the more relevant GEM signal recorded for the StCysM-peptide complex. Met1 assumes a very similar orientation in HiCysK and StCysK binding

sites. The charged terminal amino group possibly interacts with G222 backbone carbonyl while the side-chain points towards the outer part of the pocket, close to P221. The α-hydrogen, for which no signal has been observed in the difference spectrum, seems to be quite far from residues lining the pocket. A completely different orientation is assumed by Met1 when complexed with StCysM. Met1 is not involved in any specific interaction, but the side-chain is less solvent exposed and occupies a hydrophobic region delimited by M95 and P207. This different orientation is consistent with STD-NMR data, showing closer contacts between the N-terminal Met and StCysM binding site.

This interpretation of the GEM signals is further supported by the comparison between the H-bond acceptor and DRY molecular interaction fields (MIFs) for the three complexes (Figure 6, red and yellow contours), as calculated by GRID within FLAP [45]. In general, DRY fields are occupied by the hydrophobic and partially hydrophobic residues Ile4, Tyr3 and Met1, while H-bond acceptor fields are superimposed to Asp4 side-chain and to the terminal carboxylic group of Ile5. While the DRY fields are larger and present different extension and shape in the three binding sites, the H-bond acceptor fields are much more conserved, in particular in HiCysK and StCysK. Interestingly, as previously noticed, in StCysM the red contour, corresponding to the H-bond acceptor field, extends towards the PLP region and the area occupied by Ile5. This difference might contribute to explain the lower affinity measured for the MNYDI peptide towards HiCysK, with respect to StCysK and StCysM. The DRY field appears, in general, more compact in StCysK binding site and is properly occupied by Ile5, Tyr3 and also Met1, differently from the other two complexes, where an opposite orientation is assumed by Met1.

Conclusions

For all OASS isoforms here investigated the protons of the side chain of Ile5 give the largest signal in the STD spectrum, indicating that they are saturated to the highest degree. The side chain of Ile5 is thus the nearest to the active site residues and dominates the binding. This is in agreement with mutagenesis studies, where removal and/or substitution of the C-terminal Ile of CysE or peptides consistently prevent complex formation [48]. For CysM this interaction seems to give the predominant contribution to the binding energy and suggests that the larger binding site of this isoform, which binds bulkier substrates than CysK [13, 49], is not able to make strong contacts other than with the side chain of Ile5. This might explain the consistently lower affinity shown by peptides and small inhibitor molecules for CysM with respect to CysK [11, 36]. It has been suggested that the bias towards the CysK isoform might be a consequence of different interactions between the N-terminal sequence of ligand peptides and the residues lining the active site entrance

in CysK and CysM [36]. STD-NMR results confirm this observation and show closer contacts between the N-terminal Met and Asn of the pentapeptide and StCysM binding site. In the case of StCysK, that shows the highest affinity for the MNYDI peptide, a significant saturation transfer to the arylic protons is observed in the STD-NMR spectrum. In particular δH of Tyr3 contributes more than 60% to GEM. This finding is in very good agreement with the *in silico* analysis predicting a higher affinity of the peptide for StCysK, likely due to a different orientation of Tyr3 side chain.

Acknowledgments

The authors gratefully acknowledge Molecular Discovery Ltd for kindly supplying the GRID and FLAP softwares for the analysis of the proteins binding pocket.

The Interdepartment Centers SITEIA.PARMA and CIM, University of Parma, are acknowledged for the use of MALDI TOF/TOF ABSciex mass spectrometer and the NMR spectrometer, respectively.

This work is partially supported by the MSCA “INTEGRATE” 642620 within the European Union Horizon 2020 Program.

Tables

Table 1. Dissociation constant of MNYDI for HiCysK, StCysK and StCysM, in a solution containing 5 mM phosphate buffer, pH 8.0, at 20 °C.

Complex	**K_d (μM)**
HiCysK - MNYDI	109 ± 10
StCysK - MNYDI	4.4 ± 0.3
StCysM - MNYDI	275 ± 40

Table 2. ^{1}H chemical shifts (ppm) of MNYDI peptide, 50 mM phosphate buffer, pH 4.0 at 20 °C. The assignments were confirmed at pH 8.0.

Residue	**NH**	**αH**	**βH**	**others**
Met1	-	3.77	1.99, 2.09	γCH_2 2.48, 2.34 εCH_3 2.06
Asn2	8.77	4.78	2.80, 2.71	γNH_2 7.67, 6.99
Tyr3	8.37	4.65	2.88, 3.20	δH 7.18 εH 6.87
Asp4	8.46	4.70	2.76, 2.63	
Ile5	7.65	4.13	1.86	γCH_2 1.44, 1.15 γCH_3 0.91 δCH_3 0.91

References

1. Kredich, N. M. & Tomkins, G. M. (1966) The enzymic synthesis of L-cysteine in *Escherichia coli* and *Salmonella typhimurium*, *J Biol Chem.* **241**, 4955-65.

2. Droux, M., Martin, J., Sajus, P. & Douce, R. (1992) Purification and characterization of O-acetylserine (thiol) lyase from spinach chloroplasts, *Arch Biochem Biophys.* **295**, 379-90.

3. Smith, I. K. & Thompson, J. F. (1971) Purification and characterization of L-serine transacetylase and *O*-acetyl-L-serine sulfhydrylase from kidney bean seedlings (*Phaseolus vulgaris*), *Biochim Biophys Acta.* **227**, 288-95.

4. Schnell, R., Oehlmann, W., Singh, M. & Schneider, G. (2007) Structural insights into catalysis and inhibition of O-acetylserine sulfhydrylase from Mycobacterium tuberculosis. Crystal structures of the enzyme alpha-aminoacrylate intermediate and an enzyme-inhibitor complex, *J Biol Chem.* **282**, 23473-81.

5. Chinthalapudi, K., Kumar, M., Kumar, S., Jain, S., Alam, N. & Gourinath, S. (2008) Crystal structure of native O-acetyl-serine sulfhydrylase from Entamoeba histolytica and its complex with cysteine: structural evidence for cysteine binding and lack of interactions with serine acetyl transferase, *Proteins.* **72**, 1222-32.

6. Westrop, G. D., Goodall, G., Mottram, J. C. & Coombs, G. H. (2006) Cysteine biosynthesis in Trichomonas vaginalis involves cysteine synthase utilizing O-phosphoserine, *J Biol Chem.* **281**, 25062-75.

7. Bertagnolli, B. L. & Wedding, R. T. (1977) Purification and Initial Kinetic Characterization of Different Forms of O-Acetylserine Sulfhydrylase from Seedlings of Two Species of Phaseolus, *Plant Physiol.* **60**, 115-121.

8. Tai, C. H., Nalabolu, S. R., Jacobson, T. M., Minter, D. E. & Cook, P. F. (1993) Kinetic mechanisms of the A and B isozymes of O-acetylserine sulfhydrylase from Salmonella typhimurium LT-2 using the natural and alternative reactants, *Biochemistry.* **32**, 6433-42.

9. Kuske, C. R., Ticknor, L. O., Guzman, E., Gurley, L. R., Valdez, J. G., Thompson, M. E. & Jackson, P. J. (1994) Purification and characterization of O-acetylserine sulfhydrylase isoenzymes from Datura innoxia, *J Biol Chem.* **269**, 6223-32.

10. Kuske, C. R., Hill, K. K., Guzman, E. & Jackson, P. J. (1996) Subcellular Location of O-Acetylserine Sulfhydrylase Isoenzymes in Cell Cultures and Plant Tissues of Datura innoxia Mill, *Plant Physiol.* **112**, 659-667.

11. Spyrakis, F., Singh, R., Cozzini, P., Campanini, B., Salsi, E., Felici, P., Raboni, S., Benedetti, P., Cruciani, G., Kellogg, G. E., Cook, P. F. & Mozzarelli, A. (2013) Isozyme-specific ligands for O-acetylserine sulfhydrylase, a novel antibiotic target, *PLoS One.* **8**, e77558.

12. Singh, R., Spyrakis, F., Cozzini, P., Paiardini, A., Pascarella, S. & Mozzarelli, A. (2013) Chemogenomics of pyridoxal 5'-phosphate dependent enzymes, *J Enzyme Inhib Med Chem.* **28**, 183-94.

13. Maier, T. H. (2003) Semisynthetic production of unnatural L-alpha-amino acids by metabolic engineering of the cysteine-biosynthetic pathway, *Nat Biotechnol.* **21**, 422-7.

14. Nakamura, T., Kon, Y., Iwahashi, H. & Eguchi, Y. (1983) Evidence that thiosulfate assimilation by *Salmonella typhimurium* is catalyzed by cysteine synthase B, *J Bacteriol.* **156**, 656-62.

15. Filutowicz, M., Wiater, A. & Hulanicka, D. (1982) Delayed inducibility of sulphite reductase in cysM mutants of Salmonella typhimurium under anaerobic conditions, *J Gen Microbiol.* **128**, 1791-4.

16. Kroger, C., Colgan, A., Srikumar, S., Handler, K., Sivasankaran, S. K., Hammarlof, D. L., Canals, R., Grissom, J. E., Conway, T., Hokamp, K. & Hinton, J. C. (2013) An infection-relevant transcriptomic compendium for Salmonella enterica Serovar Typhimurium, *Cell Host Microbe.* **14**, 683-95.

17. Kredich, N. M., Becker, M. A. & Tomkins, G. M. (1969) Purification and characterization of cysteine synthetase, a bifunctional protein complex, from *Salmonella typhimurium*, *J Biol Chem.* **244**, 2428-39.

18. Campanini, B., Speroni, F., Salsi, E., Cook, P. F., Roderick, S. L., Huang, B., Bettati, S. & Mozzarelli, A. (2005) Interaction of serine acetyltransferase with *O*-acetylserine sulfhydrylase active site: evidence from fluorescence spectroscopy, *Protein Sci.* **14**, 2115-24.

19. Huang, B., Vetting, M. W. & Roderick, S. L. (2005) The active site of O-acetylserine sulfhydrylase is the anchor point for bienzyme complex formation with serine acetyltransferase, *J Bacteriol.* **187**, 3201-5.

20. Mino, K., Hiraoka, K., Imamura, K., Sakiyama, T., Eisaki, N., Matsuyama, A. & Nakanishi, K. (2000) Characteristics of serine acetyltransferase from Escherichia coli deleting different lengths of amino acid residues from the C-terminus, *Biosci Biotechnol Biochem.* **64**, 1874-80.

21. Mino, K., Yamanoue, T., Sakiyama, T., Eisaki, N., Matsuyama, A. & Nakanishi, K. (2000) Effects of bienzyme complex formation of cysteine synthetase from escherichia coli on some properties and kinetics, *Biosci Biotechnol Biochem.* **64**, 1628-40.

22. Salsi, E., Campanini, B., Bettati, S., Raboni, S., Roderick, S. L., Cook, P. F. & Mozzarelli, A. (2010) A two-step process controls the formation of the bienzyme cysteine synthase complex, *J Biol Chem.* **285**, 12813-22.

23. Campanini, B., Benoni, R., Bettati, S., Beck, C. M., Hayes, C. S. & Mozzarelli, A. (2015) Moonlighting O-acetylserine sulfhydrylase: New functions for an old protein, *Biochim Biophys Acta.* **1854**, 1184-93.

24. Diner, E. J., Beck, C. M., Webb, J. S., Low, D. A. & Hayes, C. S. (2012) Identification of a target cell permissive factor required for contact-dependent growth inhibition (CDI), *Genes Dev.* **26**, 515-25.

25. Singh, P., Brooks, J. F., 2nd, Ray, V. A., Mandel, M. J. & Visick, K. L. (2015) CysK Plays a Role in Biofilm Formation and Colonization by Vibrio fischeri, *Appl Environ Microbiol.* **81**, 5223-34.

26. Campanini, B., Pieroni, M., Raboni, S., Bettati, S., Benoni, R., Pecchini, C., Costantino, G. & Mozzarelli, A. (2015) Inhibitors of the Sulfur Assimilation Pathway in Bacterial Pathogens as Enhancers of Antibiotic Therapy, *Curr Med Chem.* **22**, 187-213.

27. Amadasi, A., Bertoldi, M., Contestabile, R., Bettati, S., Cellini, B., di Salvo, M. L., Borri-Voltattorni, C., Bossa, F. & Mozzarelli, A. (2007) Pyridoxal 5'-phosphate enzymes as targets for therapeutic agents, *Curr Med Chem.* **14**, 1291-324.

28. Amori, L., Katkevica, S., Bruno, A., Campanini, B., Felici, P., Mozzarelli, A. & Costantino, G. (2012) Design and synthesis of trans-2-substituted-cyclopropane-1-carboxylic acids as the first non-natural small molecule inhibitors of O-acetylserine sulfhydrylase, *MedChemComm.* **3**, 1111-1116.

29. Bruno, A., Amori, L. & Costantino, G. (2013) Computational Insights into the Mechanism of Inhibition of OASS-A by a Small Molecule Inhibitor, *Mol Inform.* **2**, 447-457.

30. Cosconati, S., Hong, J. A., Novellino, E., Carroll, K. S., Goodsell, D. S. & Olson, A. J. (2008) Structure-based virtual screening and biological evaluation of Mycobacterium tuberculosis adenosine 5'-phosphosulfate reductase inhibitors, *J Med Chem.* **51**, 6627-30.

31. Kumar, J. V. U., Poyraz, O., Saxena, S., Schnell, R., Yogeeswari, P., Schneider, G. & Sriram, D. (2013) Discovery of novel inhibitors targeting the Mycobacterium tuberculosis O-acetylserine sulfhydrylase (CysK1) using virtual high-throughput screening, *Bioorg Med Chem Lett.* **23**, 1182-6.

32. Nagpal, I., Raj, I., Subbarao, N. & Gourinath, S. (2012) Virtual screening, identification and in vitro testing of novel inhibitors of O-acetyl-L-serine sulfhydrylase of Entamoeba histolytica, *PLoS One.* **7**, e30305.

33. Paritala, H. & Carroll, K. S. (2013) New targets and inhibitors of mycobacterial sulfur metabolism, *Infect Disord Drug Targets.* **13**, 85-115.

34. Poyraz, O., Jeankumar, V. U., Saxena, S., Schnell, R., Haraldsson, M., Yogeeswari, P., Sriram, D. & Schneider, G. (2013) Structure-Guided Design of Novel Thiazolidine Inhibitors of O-Acetyl Serine Sulfhydrylase from Mycobacterium tuberculosis, *J Med Chem.* **56**, 6457-6466.

35. Salsi, E., Bayden, A. S., Spyrakis, F., Amadasi, A., Campanini, B., Bettati, S., Dodatko, T., Cozzini, P., Kellogg, G. E., Cook, P. F., Roderick, S. L. & Mozzarelli, A. (2010) Design of O-acetylserine sulfhydrylase inhibitors by mimicking nature, *J Med Chem.* **53**, 345-56.

36. Spyrakis, F., Felici, P., Bayden, A. S., Salsi, E., Miggiano, R., Kellogg, G. E., Cozzini, P., Cook, P. F., Mozzarelli, A. & Campanini, B. (2013) Fine tuning of the active site modulates specificity in the interaction of O-acetylserine sulfhydrylase isozymes with serine acetyltransferase, *Biochim Biophys Acta.* **1834**, 169-81.

37. Mori, M., Jeelani, G., Masuda, Y., Sakai, K., Tsukui, K., Waluyo, D., Tarwadi, Watanabe, Y., Nonaka, K., Matsumoto, A., Omura, S., Nozaki, T. & Shiomi, K. (2015) Identification of natural inhibitors of Entamoeba histolytica cysteine synthase from microbial secondary metabolites, *Frontiers in Microbiology.* **6**.

38. Meyer, B. & Peters, T. (2003) NMR spectroscopy techniques for screening and identifying ligand binding to protein receptors, *Angew Chem Int Ed Engl.* **42**, 864-90.

39. Pellegrino, S., Annoni, C., Contini, A., Clerici, F. & Gelmi, M. L. (2012) Expedient chemical synthesis of 75mer DNA binding domain of MafA: an insight on its binding to insulin enhancer, *Amino Acids.* **43**, 1995-2003.

40. Stehling, E. G., Sforca, M. L., Zanchin, N. I., Oyama, S., Jr., Pignatelli, A., Belluzzi, O., Polverini, E., Corsini, R., Spisni, A. & Pertinhez, T. A. (2012) Looking over toxin-K(+) channel interactions. Clues from the structural and functional characterization of alpha-KTx toxin Tc32, a Kv1.3 channel blocker, *Biochemistry.* **51**, 1885-94.

41. Delaglio, F., Grzesiek, S., Vuister, G. W., Zhu, G., Pfeifer, J. & Bax, A. (1995) NMRPipe: a multidimensional spectral processing system based on UNIX pipes, *J Biomol NMR.* **6**, 277-93.

42. Johnson, B. A. (2004) Using NMRView to visualize and analyze the NMR spectra of macromolecules, *Methods Mol Biol.* **278**, 313-52.

43. Wüthrich, K. (1986) *NMR of Proteins and Nucleic Acids*, John Wiley & Sons, Inc., Zurich.

44. Hwang, T. L. & Shaka, A. J. (1995) Water Suppression That Works. Excitation Sculpting Using Arbitrary Wave-Forms and Pulsed-Field Gradients, *J Magn Reson Ser A.* **112**, 275-279.

45. Baroni, M., Cruciani, G., Sciabola, S., Perruccio, F. & Mason, J. S. (2007) A common reference framework for analyzing/comparing proteins and ligands. Fingerprints for Ligands and Proteins (FLAP): theory and application, *J Chem Inf Model.* **47**, 279-94.

46. Angulo, J., Enriquez-Navas, P. M. & Nieto, P. M. (2010) Ligand-receptor binding affinities from saturation transfer difference (STD) NMR spectroscopy: the binding isotherm of STD initial growth rates, *Chemistry.* **16**, 7803-12.

47. Angulo, J. & Nieto, P. M. (2011) STD-NMR: application to transient interactions between biomolecules-a quantitative approach, *Eur Biophys J.* **40**, 1357-69.

48. Zhao, C., Moriga, Y., Feng, B., Kumada, Y., Imanaka, H., Imamura, K. & Nakanishi, K. (2006) On the interaction site of serine acetyltransferase in the cysteine synthase complex from *Escherichia coli*, *Biochem Biophys Res Commun.* **341**, 911-6.

49. Claus, M. T., Zocher, G. E., Maier, T. H. & Schulz, G. E. (2005) Structure of the O-acetylserine sulfhydrylase isoenzyme CysM from Escherichia coli, *Biochemistry*. **44**, 8620-6.

Figure labels.

Figure 1. Cysteine biosynthesis in bacteria. Inorganic sulphur enters the cell as sulfate, which is activated and reduced to bisulfide (top). Bisulfide is used by CysK to synthesize L-cysteine from *O*-acetylserine through a multi-step catalytic mechanism involving the coenzyme PLP (bottom).

Figure 2. Binding of MNYDI to HiCysK. a) Interaction map of MNYDI peptide with HiCysK active site. Modified from [35]. PDB code: 3IQH. b) Fluorescence emission spectra upon excitation at 412 nm of a solution containing 1 μM HiCysK, 5 mM phosphate buffer, pH 8.0, at 20 °C, and increasing concentrations of MNYDI. c) Dependence of the fluorescence emission intensity at 500 nm on the peptide concentration. Line through data points is the fit to a binding isotherm with K_d = 109 ± 10 μM.

Figure 3. STD spectrum of MDYDI-HiCysK, molar ratio 1:300 (assignment of resonances).

Figure 4. a) Group Epitope Mapping (GEM) of HiCysK (green), StCysM (cyan) and StCysK (blue) in complex with MNYDI peptide. The saturation of individual protons was normalized to the highest saturated proton in the peptide. b) GEM represented on the peptide structure.

Figure 5. Docking poses for the MNYDI peptide within HiCysK (**a**), StCysK (**b**) and StCysM (**c**) binding site. The peptide and the interacting residues lining the pocket are labelled and shown in capped sticks. Hydrogen bonds are displayed as black dashed lines.

Figure 6. Molecular Interaction Fields calculated for the three complexes HiCysK (**a, a'**), StCysK (**b, b'**) and StCysM (**c, c'**). For clarity only H-bond acceptor (red contours in panels on the left) and DRY (yellow contours in panels on the right) fields are reported.

Figure 1

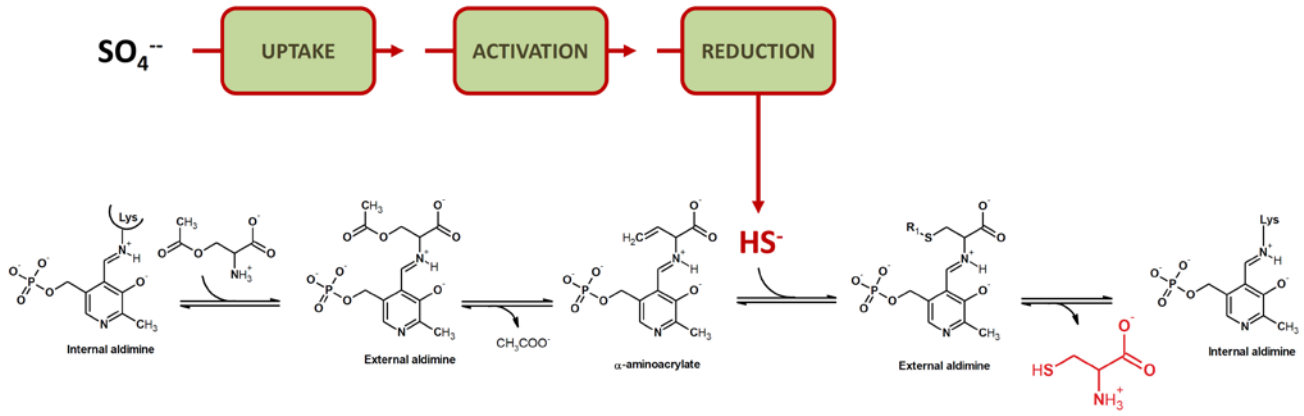
SO4--
UPTAKE
ACTIVATION
REDUCTION
HS-
Lys
Internal aldimine
External aldimine
CH3COO-
α-aminoacrylate
External aldimine
Lys
Internal aldimine
HS
NH3+

Figure 2

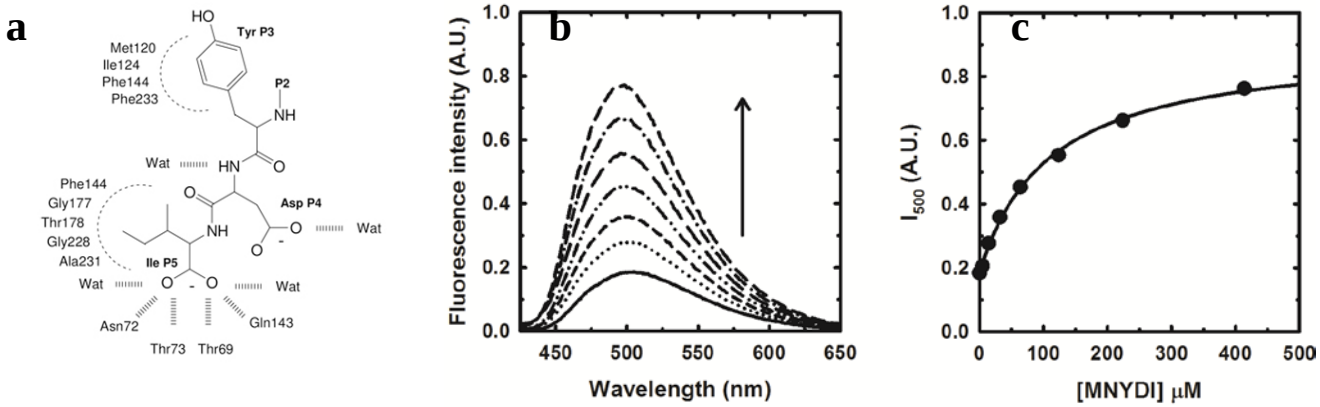
a
HO
Tyr P3
Met120
Ile124
Phe144
Phe233
P2
NH
Wat
HN
O
Phe144
Gly177
Thr178
Gly228
Ala231
Asp P4
NH
O
Wat
Ile P5
Wat
O
O
Wat
Asn72
Thr73
Thr69
Gln143
b
Fluorescence intensity (A.U.)
1.0
0.8
0.6
0.4
0.2
0.0
450
500
550
600
650
Wavelength (nm)
c
I_{500} (A.U.)
1.0
0.8
0.6
0.4
0.2
0.0
0
100
200
300
400
500
[MNYDI] μM

Figure 3

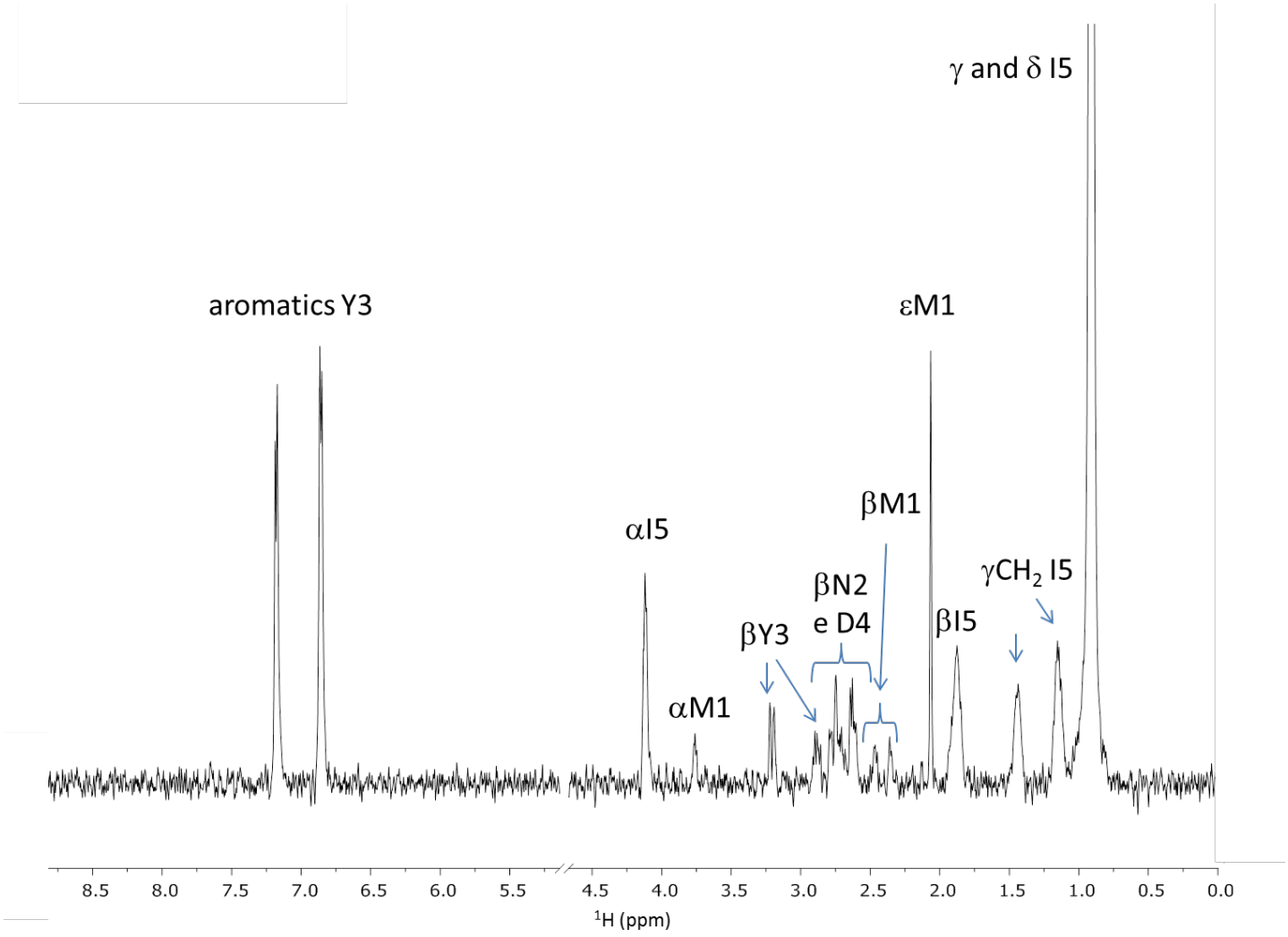
γ and δ I5
aromatics Y3
εM1
αI5
βM1
βN2
e D4
βY3
γCH2 I5
βI5
αM1
8.5
8.0
7.5
7.0
6.5
6.0
5.5
4.5
4.0
3.5
3.0
2.5
2.0
1.5
1.0
0.5
0.0
1H (ppm)

Figure 4

a

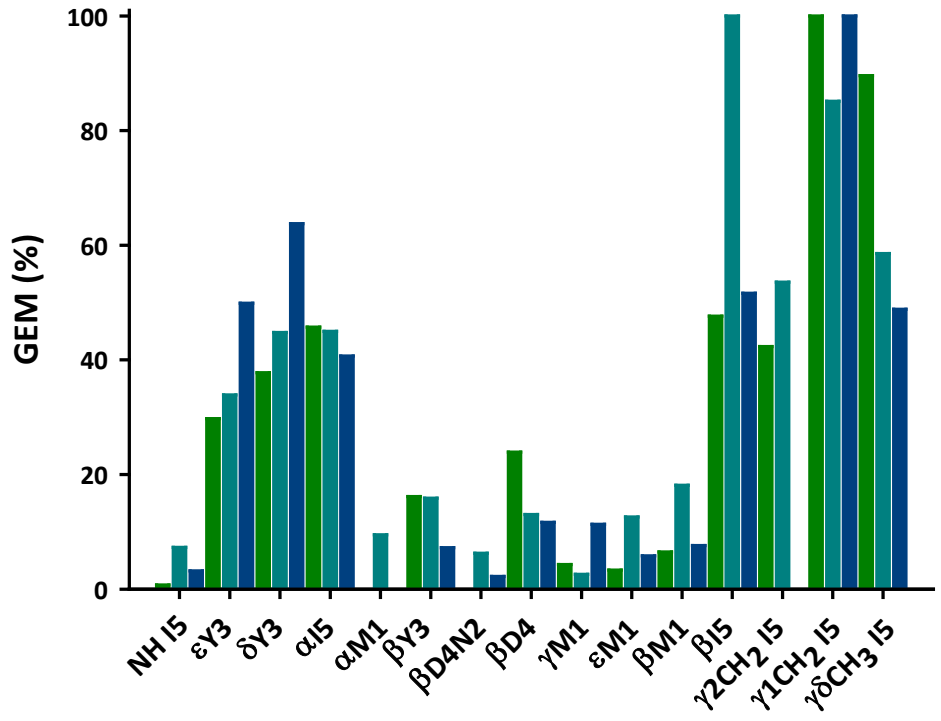
GEM (%)
100
80
60
40
20
0
NH I5
εγ3
δγ3
αI5
αM1
βγ3
βD4N2
βD4
γM1
εM1
βM1
βI5
γ2CH2 I5
γ1CH2 I5
γδCH3 I5

b

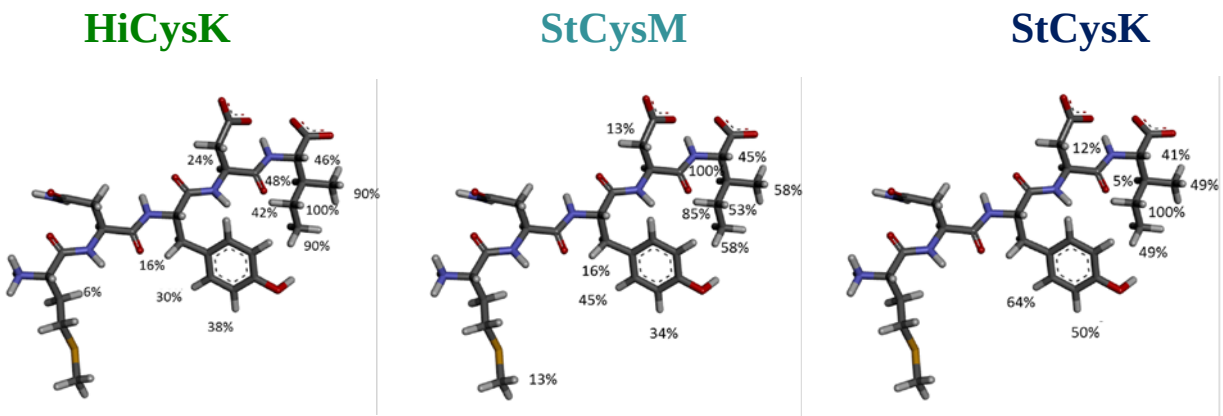
HiCysK
StCysM
StCysK
24%
46%
48%
90%
42%
100%
90%
16%
6%
30%
38%
13%
45%
100%
58%
85%
53%
58%
16%
45%
34%
13%
12%
41%
5%
49%
100%
49%
64%
50%

Figure 5

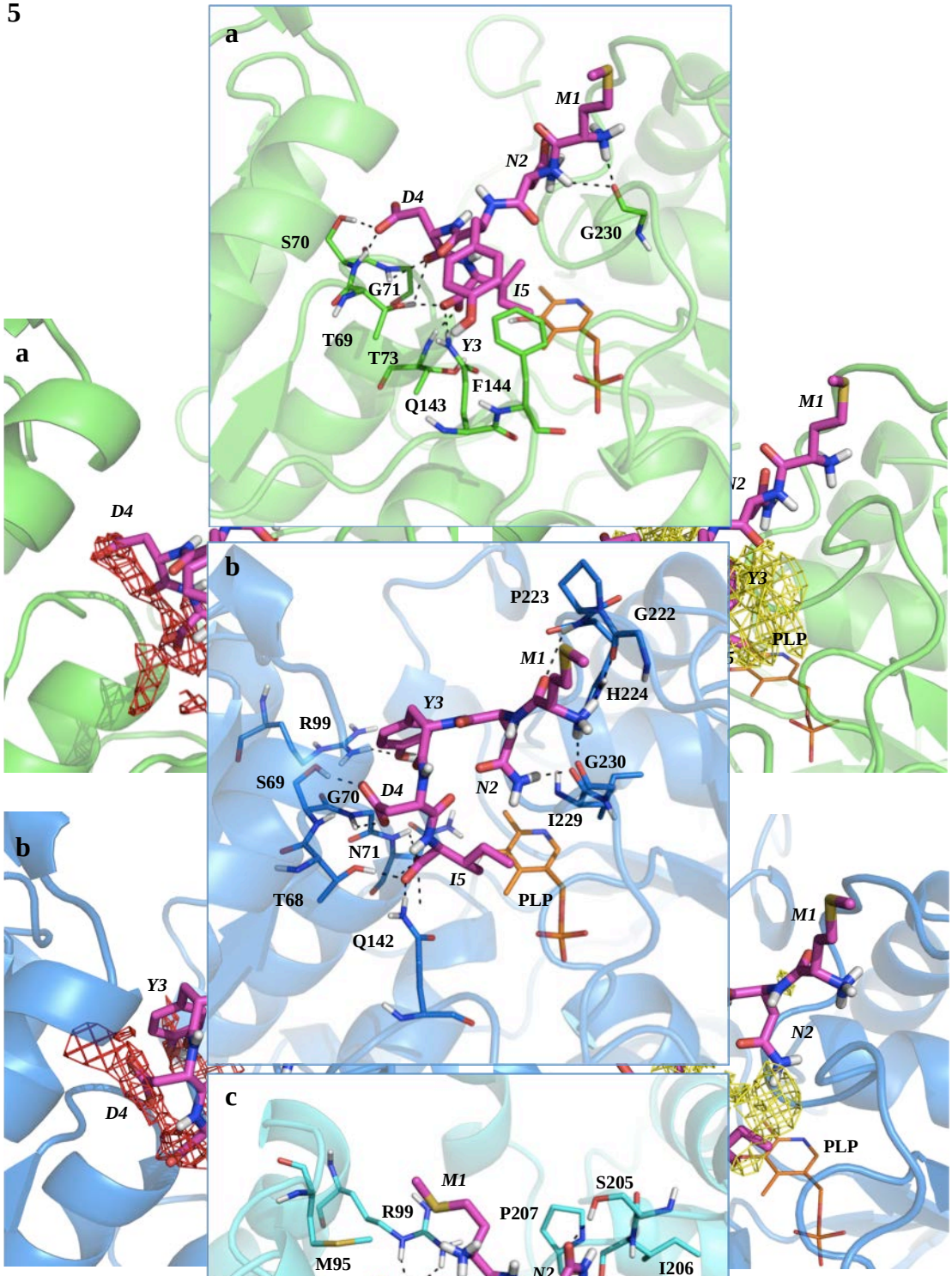

Figure 6

Supplementary Material

Figure S1.

1D NMR spectrum of 400 μM StCysM, 5 mM phosphate buffer, pH 8.0, 20 °C.

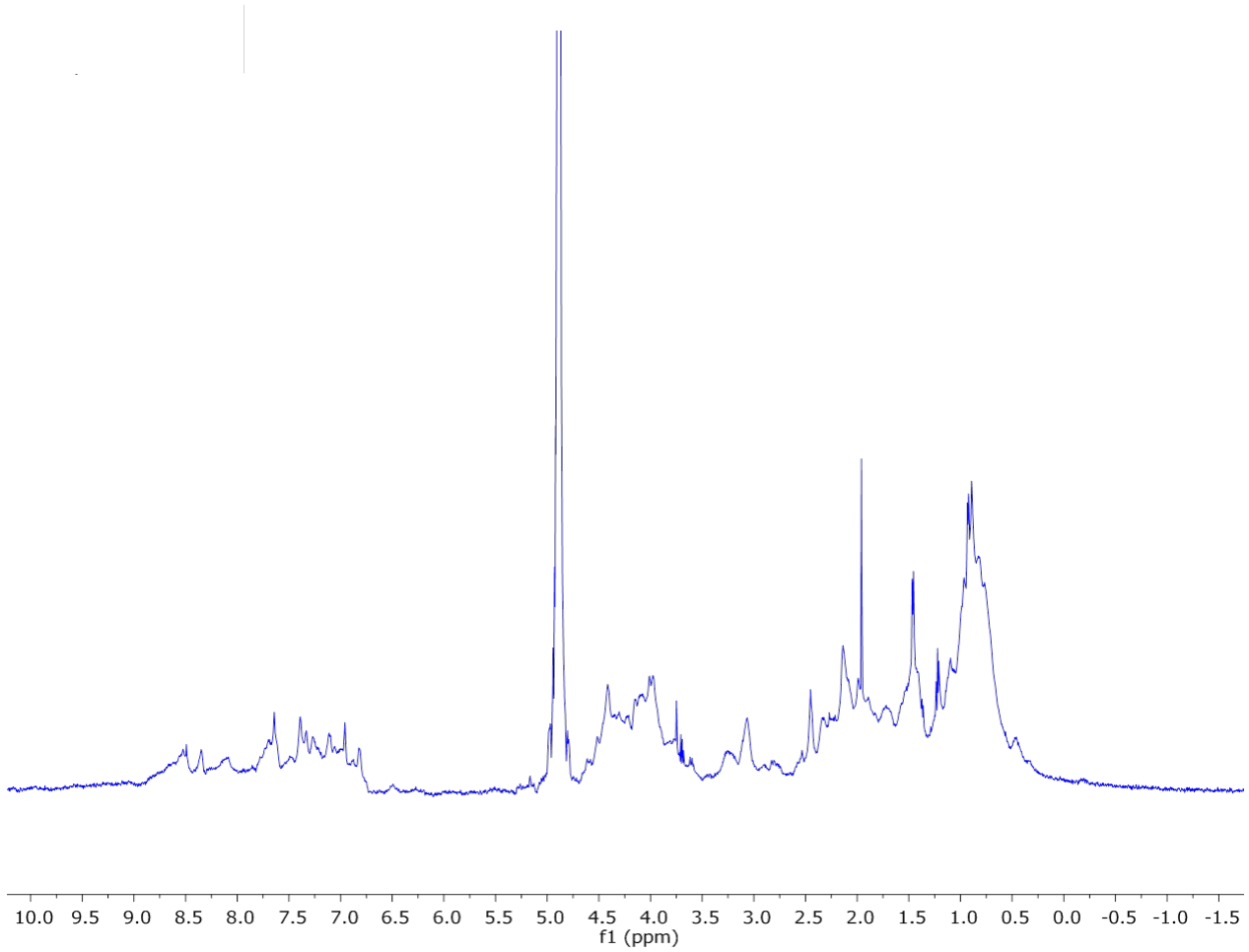

Figure S2.

STD-NMR experiments.

Panel a. Off-resonance spectrum of MNYDI-HiCysK*.

Panel b. On-resonance spectrum of MNYDI alone.

Panel c. STD spectrum of HiCysK/MNYDI complex.

Panel d. STD spectrum of StCysK/MNYDI complex.

Panel e. STD spectrum of StCysM/MNYDI complex.

*For visualization reasons the off resonance spectrum is attenuated 100x.

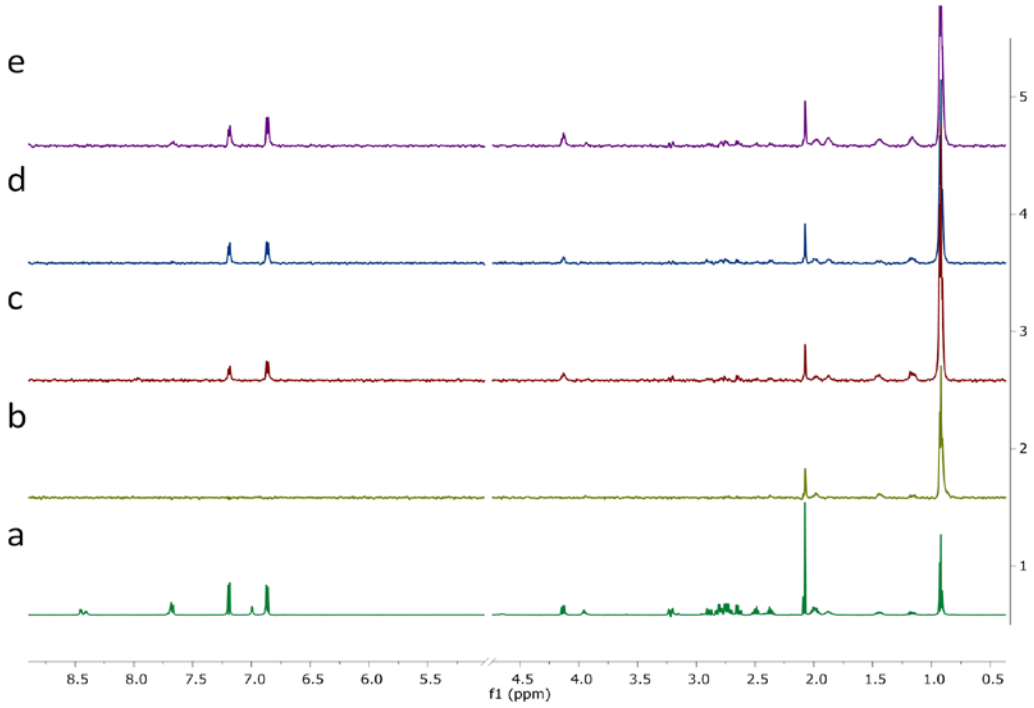
e
d
c
b
a
5
4
3
2
1
8.5
8.0
7.5
7.0
6.5
6.0
5.5
4.5
4.0
3.5
3.0
2.5
2.0
1.5
1.0
0.5
f1 (ppm)